PHYSICAL REVIEW B VOLUME 15, NUMBER 6 15 MARCH 1977

# Comparative study of the electronic structure of noble-metal–noble-metal alloys by optical spectroscopy*

Josette Rivory
*Laboratoire d'Optique des Solides, Université Paris VI, Paris Cedex 05, France*
(Received 5 April 1976)

Transmittance and reflectance measurements have been performed between 0.5 and 6 eV on thin films of noble-metal–noble-metal alloys over the whole concentration range. Optical absorption clearly shows that these alloys are of two types: On the one hand, in Au-Ag and Au-Cu alloys, the absorption spectrum moves and modifies its shape gradually from a constituent to the other one; on the other hand, in Ag-Cu alloys, the absorption spectrum has essentially the shape of the matrix spectrum, with a supplementary absorption band due to impurities. This suggests that in the first case, the *d* bands of the constituents strongly overlap, while in the second case they overlap only slightly. All these results will be discussed in the framework of existing theories: the coherent-potential approximation and the virtual-bound-state theory. Ordering effects in Au-Cu and clustering effects in Ag-Cu are also investigated.

## I. INTRODUCTION

The electronic structure of disordered alloys is now fairly well understood. The coherent-potential approximation[1,2] (CPA), which has recently been considerably developed, proves to be valid for high concentrations and strong scattering and therefore provides a link between the two limiting cases treated previously: the weak-perturbation limit, well described, for example, in the virtual crystal model,[3] and the low-concentration limit for strong perturbation, also described in the virtual-bound-state model.[4,5] Investigations on the three series of binary alloys involving noble metals appear to be interesting, because these alloys present different strengths of perturbation, and are tractable from a theoretical point of view, which permits a test of the theory in different cases.

Indeed, these alloys have quite different behaviors, in particular their phase diagrams show basic differences.[6] Au and Ag form solid solutions over the whole concentration range, which crystallize in the fcc system like the pure metals. The same is true for the Au-Cu system, but over certain composition ranges, ordered phases can be obtained, corresponding to AuCu (I and II) between 35- and 65-at.% Cu, $AuCu_3$ (I and II) between 65- and 80-at.% Cu, and $Au_3Cu$ around 25-at.% Cu. In addition, the lattice parameters of Au and Ag are very similar, whereas those of Au and Cu are different; for Au-Cu alloys, volume effects will add to potential effects. Eventually, the Ag-Cu system presents a solubility anomaly with respect to the semiempirical Hume-Rothery rule; the phase diagram shows a simple eutectic, with comparison 39.9-at.% Cu the solubility being negligible below 200 °C. At higher temperatures, the solubility never exceeds 10% at both ends of the diagram. However, Ag-Cu solid solutions can be obtained in metastable state by liquid or vapor quenching. This last method has been used in the present work.

There has been little previous systematic investigation of the optical properties of noble-metal–noble-metal alloys over the whole concentration range. Pioneering work was done on Au-Ag alloys by Wessel,[7] Fukutani and Sueoka,[8] Fukutani,[9] and also by McAlister *et al.*,[10] who investigated the alloy Fermi surface by Faraday-effect measurements. Nilsson[11] performed optical and photoemission measurements on Ag-Au and Cu-Au alloys in disordered phases. Nilsson and Norris,[12] Stahl *et al.*[13] and Scott and Muldawer[14] investigated the influence of compositional ordering on the optical properties of Au-Cu alloys in the case of the $AuCu_3$ superlattice. Preliminary results on Ag-Cu alloys were presented recently by Nilsson and Forsell.[15] Beaglehole[16] performed a detailed comparative study of the three disordered alloy series only in the very dilute case (<1%), using differential reflectance measurements. Most of these papers gave information essentially on interband transitions. Only Beaglehole[16] deduced values of the optical effective mass from his measurements in a spectral range where the leading contribution was from interband transitions.

This paper presents the results of systematic investigations on the optical properties of noble-metal–noble-metal binary alloys over the whole concentration range, taking into account both conduction electrons and interband transitions. Attention is given to concentration characterization (after deposition) and to sample structure and homogeneity. This is important especially for the Au-Cu series because of the existence of ordered phases stable at room temperature, and for the Ag-Cu series because of the lack of solubility,

which can lead to clustering and phase separation.

From a theoretical point of view, our results on disordered alloys will be tentatively interpreted in the framework of the CPA. Drastic differences will show up between the optical behavior of Au-Ag and Au-Cu on the one hand, and Ag-Cu on the other hand, concerning especially the variation of the interband absorption onset with alloying. In order to explain these experimental results, a scheme will be proposed to describe the relative positions of the *d* bands of the constituents, following an argument developed by Gelatt and Ehrenreich[17] for Au-Ag alloys. It will be inferred that in Au-Ag and Au-Cu alloys, the *d* bands of the two constituents strongly overlap, whereas in Ag-Cu alloys, they overlap only partially, retaining their individuality in the alloy.

For dilute Ag-Cu alloys, the concept of the virtual-bound state will also be used to analyze the optical data quantitatively. The position and width of the *d* levels on Cu impurities in an Ag matrix will be determined.

Moreover, the influence of compositional ordering on optical absorption in the case of the AuCu and $AuCu_3$ superlattices will be determined. The effect of partial and complete phase separation in Ag-Cu alloys will be investigated. The results will show that the partial *d* density of states is sensitive to the local atomic environment.

In Sec. II, the experimental methods will be characterized briefly. In Sec. III, the experimental results obtained for disordered alloys will be described, as well as the effect of compositional ordering in the case of Au-Cu. Finally, in Sec. IV, the data will be compared and discussed using various theoretical models of the electronic structure of metallic alloys.

## II. EXPERIMENT

Semitransparent thin alloy films (200–400 Å thick) were deposited in an oil-pumped vacuum system ($10^{-7}$ Torr) by coevaporation of the two constituents from the same tungsten crucible onto amorphous silica substrates held at room temperature, except for Ag-Cu alloys which were deposited on substrates at low temperature.

Film thickness was determined by x-ray interferences in reflection with 1% accuracy.[18] For Au-Cu alloys, the concentration can be deduced from the displacement of the x-ray (111) diffraction peak, because the variation of the lattice parameter on alloying is large enough[19] and the annealed films are made of large and well-oriented crystallites [the (111) reticular planes being parallel to the substrate surface]. This method cannot be used in the two other cases: for Ag-Au, because the lattice parameter changes very little with composition; for Ag-Cu, because the films are made of misoriented microcrystallites. In all cases, the alloy concentration can be determined by electron microprobe analysis[20] with a few percent accuracy.

Heat treatments are different according to the series under investigation. (i) Au-Ag alloys were carefully annealed *in situ*, in order to obtain good samples with large crystals, whose properties are as close as possible to the bulk properties. The film recrystallization was controlled by simultaneous measurements of the electrical resistivity. (ii) As-deposited Au-Cu alloy films were always disordered. This disordered phase is stable at room temperature outside the concentration ranges where superlattices can be formed, but metastable inside these ranges. In the latter case, evidence for short-range order only can be detected in these as-deposited disordered alloys.[21,22] By annealing, recrystallization takes place together with the formation of the superlattice.[22] Above the order-disorder transition temperature (which depends on concentration), a disordered phase can be obtained again, which is then stable and well crystallized. This phase can, in principle, be maintained metastable at room temperature by quenching the film. In practice, it is very difficult to avoid some ordering during this process. Therefore, we systematically chose to study the disordered phases just after deposition, although they consisted of very small crystallites. (iii) Metastable Ag-Cu solid solutions were obtained by deposition on substrates held at low temperature (120 °K). These alloys were warmed up to room temperature for optical measurements without noticeable modification of their structure. Annealing at higher temperature produced gradual impurity clustering and eventually phase separation of the two constituents.[23]

The film structure was carefully investigated by electron microscopy and electron diffraction. Crystal sizes are typically 3000 to 5000 Å for Au-Ag and Au-Cu annealed films and about 15 Å for microcrystalline Ag-Cu films. Microdensitometer analysis of electron diffraction patterns gives information on crystallite orientation, alloy homogeneity (existence of a single or of several phases), short- and long-range order. This permits the evaluation of the long-range order parameter for samples where the AuCu or $AuCu_3$ superlattice can be formed. The optical constants of the films between 0.5 and 6 eV are deduced from transmittance and reflectance measurements at nearly normal incidence, the film thickness being known.[24]

## III. DESCRIPTION OF THE OPTICAL DATA

In the following, we will essentially consider the modifications with alloying of the complex dielectric function $\tilde{\epsilon}(\omega) = (n+ik)^2 = \epsilon_1 + i\epsilon_2$, which represents the response of the medium to the incident electromagnetic wave. It is assumed that this quantity can be written as the sum of two terms[25]: $\epsilon^{(D)}(\omega)$ corresponding to intraband transitions of conduction electrons, and $\epsilon^{(i)}(\omega)$ corresponding to interband transitions. For the noble metals and their alloys, the onset of interband transitions $\omega_0$ is always greater than 2 eV and therefore the dielectric constant in the infrared region ($0.5 < \omega < 1.2$ eV) essentially reduces to the intraband contribution. It will be analyzed according to the Drude theory, some slight modifications being made to take into account effects such as electron-electron interactions, influence of lattice imperfections, etc.

### A. Disordered alloys

#### *1. Intraband transitions*

The dielectric constant in the range of intraband transitions can be described by

$$\epsilon_1 = \epsilon_1^{(D)} + 4\pi\alpha_0 + \delta\epsilon_1^{(i)} , \tag{3.1a}$$

$$\epsilon_2 = \epsilon_2^{(D)} \tag{3.1b}$$

where $\epsilon^{(D)} = \epsilon_1^{(D)} + i\epsilon_2^{(D)}$ is the Drude formula for the dielectric constant,[26] $4\pi\alpha_0$ represents the core polarization and $\delta\epsilon_1^{(i)}$ is the contribution of the interband transitions, which can be deduced from the interband absorption $\epsilon_2^{(i)}$ by the Kramers-Krönig transformation

$$\delta\epsilon_1^{(i)}(\omega) = \frac{2}{\pi}\int_{\omega_0}^{\infty} \frac{\omega'\epsilon_2^{(i)}(\omega')\,d\omega'}{\omega'^2 - \omega^2} , \tag{3.2}$$

$\omega_0$ being the threshold of interband transitions. For energies $\omega \ll \omega_0$, $\delta\epsilon_1^{(i)}$ can be considered as a constant term. The following expressions will thus be used:

$$\epsilon_1(\omega) = P - \omega_p^2\tau^2/(1+\omega^2\tau^2) , \tag{3.3a}$$

$$\epsilon_2(\omega) = \omega_p^2\tau/\omega(1+\omega^2\tau^2) . \tag{3.3b}$$

Here $\omega_p$ is the plasma frequency of the conduction electrons, defined by $\omega_p^2 = 4\pi Ne^2/m^* = 4\pi N_{\text{eff}}e^2/m$, $m^*$ and $N_{\text{eff}}$ being, respectively, the optical effective mass and the effective number of conduction electrons; $\tau$ is the optical relaxation time. For pure metals, $\omega\tau \gg 1$ (even at $\omega = 0.5$ eV), thus one can write:

$$\epsilon_2(\omega) \approx \omega_p^2/\omega^3\tau . \tag{3.4}$$

In an earlier study,[27] it was noted that it was necessary to add to this expression of $\epsilon_2$ a term proportional to $\omega^{-1}$ in order to correctly represent the experimental results. This term can be accounted for, if it is assumed that the relaxation time varies with frequency as

$$\tau^{-1}(\omega) = \tau^{-1}(0) + b\omega^2 , \tag{3.5}$$

where $b$ is a constant.[27,28] In the alloy case, for which the relaxation time can be much shorter, we cannot always neglect 1 compared to $\omega^2\tau^2$ and the set of expressions (3.3) must be used, with a term $A/\omega$ added to $\epsilon_2(\omega)$. The four parameters $A, P, \omega_p, \tau$ are determined by a least-square fitting to the experimental values of $R$ and $T$.

The optical effective mass $m^*$ can be deduced from the values of the plasma frequency $\omega_p$ assuming one conduction electron per atom. For Au-Ag alloys, the number of atoms per unit volume $N$ does not change with concentration; however, for Au-Cu and Ag-Cu alloys, the variation of the lattice parameter with concentration $a(x)$ has to be taken into account. The values of $a(x)$ quoted in the literature[19] for Au-Cu alloys show a positive deviation with respect to Vegard's law. In the case of Ag-Cu alloys, few experimental values are available[29,30] and we have assumed the same variation as for Au-Cu alloys.

The shape of the curves giving the optical mass versus concentration obviously depends on the values chosen for the pure metals which are still under discussion; we have taken the values reported in Table I. Figures 1(a), 1(b), and 1(c) show the results obtained for the three series of alloys. The dispersion of these results is large; as a matter of fact, the accuracy in the determination of the optical mass is strongly related to the accuracy on thickness and transmission measurements. In our experiments, the error on thickness is small (about 1%), but the error on transmission measurements in the infrared region may be important for the thickest films under investigation. In Table I, we only indicate the sign

TABLE I. Optical effective mass $m^*$ for Au, Ag, Cu, and relative variation $\Delta m^*/m^*$ with 1-at.% impurity for the three-alloy series.

| | $m^*$ | | $\frac{\Delta m^*}{m^*}$ [a] | $\frac{\Delta m^*}{m^*}$ [b] |
|---|---|---|---|---|
| Au | 0.94 [c] | *Au*–Ag | $<0$ | $-0.004 \pm 0.003$ |
| | | *Au*–Cu | $\lesssim 0$ | $-0.004 \pm 0.002$ |
| Ag | 0.89 [d] | *Ag*–Au | $<0$ | $-0.011 \pm 0.007$ |
| | | *Ag*–Cu | $>0$ | $0.013 \pm 0.010$ |
| Cu | 1.40 [a] | *Cu*–Au | $<0$ | $-0.002 \pm 0.005$ |
| | | *Cu*–Ag | $<0$ | $-0.004 \pm 0.014$ |

[a] This work. [c] Reference 27.
[b] Reference 16. [d] Reference 31.

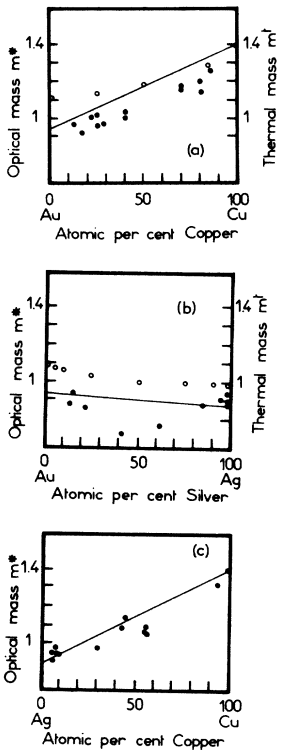


FIG. 1. Variation vs concentration of the optical effective mass $m^*$(●) for Au-Cu (a), Au-Ag (b), Ag-Cu (c) alloys and of the thermal effective mass $m_t$ (○) for Au-Cu (a) and Au-Ag (b) alloys. The lines represent linear interpolations between the pure metal values.

of the relative variation of the optical mass for one atomic percent impurity: $\Delta m^*/m^*$. For comparison, we also give the corresponding values deduced by Beaglehole[16] from differential optical measurements performed in an energy range ($\omega > 1.5$ eV) where one has to take into account a strong contribution of interband transitions. The agreement is qualitatively good, except for *Au*-Cu alloys, for which we find practically no variation of $m^*$ for very dilute alloys; however, it is worth noting that the values chosen by Beaglehole for $m^*$ in pure Au and pure Cu are slightly different from ours: 0.97 and 1.45, respectively (instead of 0.94 and 1.40). Due to the dispersion of our results, one cannot expect to obtain quantitative agreement. In conclusion, in Au-Ag and Au-Cu alloys a negative deviation with respect to the linear interpolation between the values of the two pure constituents is the most likely behavior for the optical mass; on the contrary, in Ag-Cu alloys the variation of $m^*$ seems much closer to a linear variation.

It is interesting to compare the variation with concentration of the optical effective mass $m^*$ with the variation of the thermal effective mass $m_t$. $m_t$ is deduced from low-temperature specific-heat measurements: $m_t = \gamma/\gamma_0$, where $\gamma$ is the electronic specific-heat coefficient and $\gamma_0$ its value for the corresponding free electron gas. The optical mass is related to the average velocity on the Fermi surface and the thermal mass to the average reciprocal velocity[26]:

$$m_t/m^* = (S_F/S_F^0)^2 \langle v \rangle \langle 1/v \rangle \ , \tag{3.6}$$

where $S_F$ and $S_F^0$ are the areas of the real Fermi surface and of the equivalent free-electron Fermi sphere, respectively. In Figs. 1(a) and 1(b), we have shown the variation of $m_t$ for Au-Cu alloys from the results of Martin and Waterhouse[32] and for Au-Ag alloys from the results of Davis and Rayne.[33] These curves clearly show an analogy with the variations of $m^*$. As confirmed by positron annihilation experiments in pure Cu and disordered $AuCu_3$ alloy,[34] the alloy Fermi surface must be more spherical than the pure metal one, due to disorder. One might expect the ratio $m_t/m^*$ to be closer to unity in alloys than in the pure constituents. However, one has also to take into account the variation of the Fermi surface area on alloying, since its contact areas with the boundaries of the Brillouin zone are also modified. Therefore it is difficult to draw any definite conclusion.

As previously mentioned, the optical relaxation time has to be assumed frequency dependent in alloys as well as in pure metals. In the case of pure metals, it was qualitatively shown that the amplitude of this variation can be related to the crystallographic structure of the samples.[27] As will be discussed further below, such behavior has been interpreted within the framework of the CPA in both cases as due to disorder effects. The reciprocal relaxation time at zero frequency $\tau^{-1}(0)$ shows a Nordheim-type variation with concentration like the dc electrical resistivity. The values of $\tau^{-1}(0)$ are strongly dependent on the sample history. Typical values obtained for pure metals and for 50-at.% alloys are summarized in Table II. The smallest amplitude of variation with concentration is observed for Ag-Cu alloys.

TABLE II. Typical values of the reciprocal relaxation time for Ag, Cu, Au, and their three 50-at.% alloys.

| | $\tau^{-1}(0)$ (sec$^{-1}$) | | $\tau^{-1}(0)$ (sec$^{-1}$) |
|---|---|---|---|
| Ag | (4 to 8)$\times 10^{13}$ | Ag–50-at.% Cu | $2\times 10^{14}$ |
| Cu | (8 to 9)$\times 10^{13}$ | Ag–50-at.% Au | $3\times 10^{14}$ |
| Au | (6 to 8)$\times 10^{13}$ | Au–50-at.% Cu | $3.8\times 10^{14}$ |

### 2. *Interband transitions*

Figures 2–4 show the variation of the interband transition contribution to the imaginary part of the dielectric constant $\epsilon_2^{(i)}(\omega)$ versus energy for Au-Ag, Au-Cu, and *Cu*-Ag alloys, respectively, and Fig. 5 shows the imaginary part of the total dielectric constant $\epsilon_2(\omega)$ for *Ag*-Cu alloys. $\epsilon_2^{(i)}(\omega)$ is obtained from $\epsilon_2(\omega)$ by subtracting the conduction electron contribution calculated from the values of the characteristic parameters $m^*$ and $\tau$ as determined in the infrared. These figures show an analogy between the two series Au-Ag and Au-Cu, in which a gradual deformation of the curves and a continuous shift of the absorption edge with concentration over the entire range are observed. For the Ag-Cu series, the situation is quite different: one must distinguish the *Cu*-Ag case for which one observes essentially the spectrum of pure Cu and a broadening rather than a shift of the absorption edge, from the *Ag*-Cu case, for which the behavior is very close to the one in pure Ag, except for a distinct supplementary contribution due to Cu impurities.

In the Au-Ag series, for increasing Ag concentration, one observes a shift towards higher energies and a gradual broadening of the absorption edge, whereas the second maximum of the pure Au spectrum, located at 3.9 eV, remains at the same position up to about 20-at.% Ag. For higher concentration, this maximum is less and less apparent. Eventually, for 60-at.% Ag, the shape of the spectrum resembles that of pure Ag; however, the edge is at lower energies and much broader than in pure Ag. It is seen that the absorption edge moves much more rapidly when Au is added to Ag than in the opposite situation when Ag is added to Au.

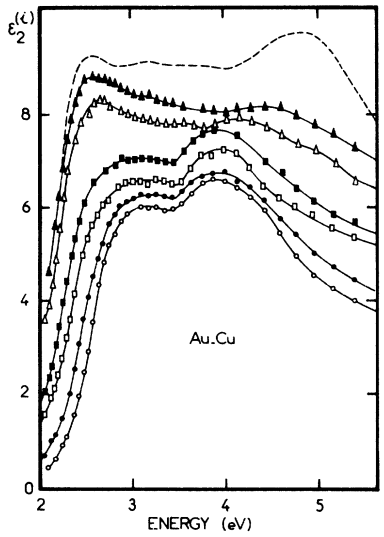


FIG. 3. Imaginary part of the interband dielectric constant $\epsilon_2^{(i)}$ vs energy for Au-Cu alloys with Cu concentrations in at.%: 12 (●), 25 (□), 40 (■), 70 (△), 81 (▲), for pure Au (○) and pure Cu(---), arbitrarily shifted.

In the Au-Cu series, one sees again the gradual shift of the absorption edge from Au to Cu (in Fig. 3, the $\epsilon_2^{(i)}(\omega)$ curves have been arbitrarily shifted upwards for clarity). One notes that the second maximum centered at about 3.9 eV in pure Au seems to remain practically unmodified up to large Cu concentration (about 40-at.% Cu). By contrast, the absorption maximum located at 5 eV

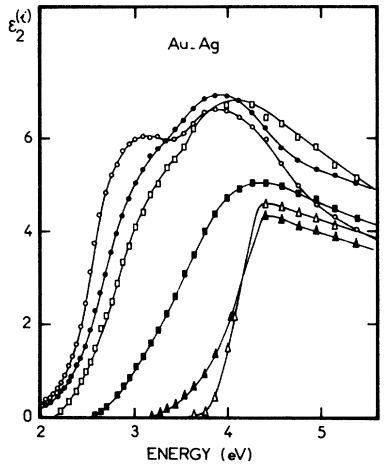


FIG. 2. Imaginary part of the interband dielectric constant $\epsilon_2^{(i)}$ vs energy for Au-Ag alloys with Ag concentrations in at.%: 21 (●), 41 (□), 62 (■), 94 (▲) for pure Au (○) and pure Ag (△).

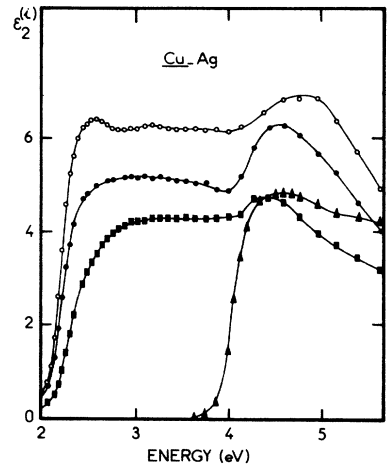


FIG. 4. Imaginary part of the interband dielectric constant $\epsilon_2^{(i)}$ vs energy for *Cu*-Ag alloys, with Cu concentrations in at.%: 55 (■), 94 (●) and for pure Cu (○) and pure Ag (▲).

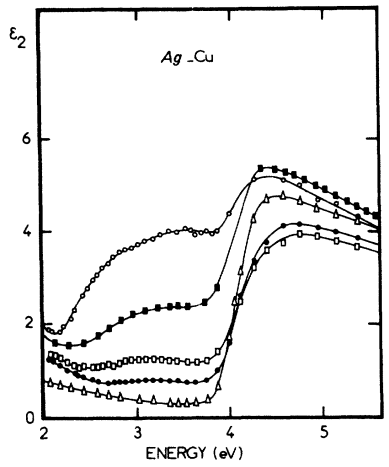


FIG. 5. Imaginary part of the total dielectric constant $\epsilon_2$ vs energy for *Ag*-Cu alloys with Cu concentrations in at.%: 6 (●), 8 (□), 30 (■), 43 (○) and for pure Ag (Δ).

in the spectrum of pure Cu moves towards smaller energies and disappears rapidly when Au is added to Cu. A similar shift of this peak towards smaller energies is also observed in Fig. 4 when Ag is added to Cu. The well-defined maximum seen for the Cu–45-at.%-Ag alloy at about 4.3 eV is an interesting feature, which can either be related to the transformation of a feature of the pure Cu or Ag spectra, or be considered as a new feature characteristic of the alloy.

As shown in Fig. 5, for the *Ag*-Cu alloys, the $\epsilon_2(\omega)$ curves consist roughly in the interband absorption spectrum of pure Ag, only slightly modified, together with a supplementary absorption peak located at energies lower than the threshold of interband transitions of pure Ag. This absorption increases with Cu concentration, while it remains centered at about 3.2 eV. When the Cu concentration increases, the curve changes its shape and becomes less symmetrical; its low-energy part is steeper and turns into an absorption edge. In Sec. IV, it will be shown that this absorption in dilute *Ag*-Cu alloys due to *d* levels of Cu impurity in Ag can be analyzed in terms of the virtual-bound-state model.

We will now investigate quantitatively the variation of the interband absorption onset $\omega_0$ with concentration. $\omega_0$ should be defined as the frequency for which $\epsilon_2^{(i)}(\omega)$ becomes different from zero. In pure noble metals, the determination of $\omega_0$ is not straightforward, in particular, because of the existence of absorption tails at $\omega<\omega_0$. In alloys the extrapolation of $\epsilon_2^{(i)}(\omega)$ is even more difficult because the shape of the edge changes with concentration. In some cases, the joint density of states: $J(\omega)=\omega^2$. $\epsilon_2^{(i)}(\omega)$ (if matrix elements are

TABLE III. Absorption onset $\omega_0$ for Au, Ag, Cu as determined from extrapolation of the joint density of states $J(\omega)$ and from the imaginary part of the interband dielectric constant $\epsilon_2^{(i)}(\omega)$.

| | $\omega_0\,[J(\omega)]$ | $\omega_0\,[\epsilon_2^{(i)}(\omega)]$ |
|---|---|---|
| Au | 2.45 [a] | 2.50 |
| Cu | 2.08 [b] | 2.20 |
| Ag | 3.87 [c] | 4.08 |

[a] Reference 27.
[b] This work.
[c] Reference 31.

assumed to be constant) can be fitted with a simple analytic expression. For pure Au, Theye[27] showed that $J(\omega)$ at the edge has a parabolic behavior over a relatively large energy range. By linear extrapolation of $J^2(\omega)$, $\omega_0$ can easily be obtained. For pure Ag, $J(\omega)$ can be considered as linear in the region of the absorption edge. This is also the case for pure Cu, though in a smaller energy range. In order to use a definition of $\omega_0$ valid over the whole concentration range (in particular in the case of Au-Cu) we also tried to define $\omega_0$ as the frequency for which $\epsilon_2^{(i)}(\omega)$ reaches half of the value of its first maximum. The results obtained by these two definitions: extrapolation of $J(\omega)$ and half-height of the maximum in $\epsilon_2^{(i)}(\omega)$ lead to the same conclusions, but the values of $\omega_0$ are slightly higher in the latter case, as shown in Table III.

Figure 6(a) represents the variation of $\omega_0$ versus concentration for Au-Ag alloys. To determine $\omega_0$,

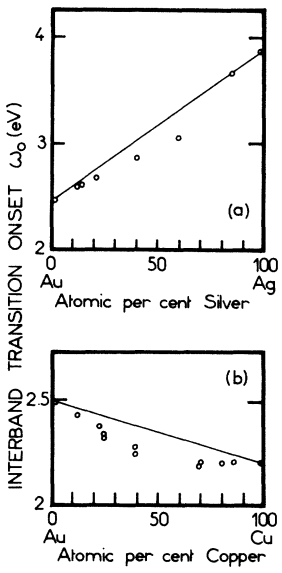


FIG. 6. Variation of the interband transition onset $\omega_0$ versus concentration for Au-Ag (a) and Au-Cu (b) alloys. The lines represent linear interpolations between the pure metal values.

we choose to extrapolate $J^2(\omega)$ for Au-rich alloys and $J(\omega)$ for Ag-rich alloys, because the first maximum in $\epsilon_2^{(i)}(\omega)$ is not well defined in Au-rich alloys. Figure 6(b) represents $\omega_0(x)$ values for Au-Cu alloys; here $\omega_0$ is obtained from $\epsilon_2^{(i)}(\omega)$. In the two series we find the same qualitative variation, i.e., a negative deviation with respect to the linear interpolation between the values of the pure constituents. The remarks made above when considering the $\epsilon_2^{(i)}(\omega)$ curves are confirmed: the absorption onset moves more rapidly in *Ag*-Au and *Au*-Cu than in *Au*-Ag and *Cu*-Au, respectively.

For Ag-Cu alloys, the situation is quite different. For Ag-rich alloys, we calculated the joint density of states $J(\omega)$ corresponding to pure Ag by subtracting from $\epsilon_2(\omega)$ the contribution of conduction electrons and the supplementary absorption due to Cu impurity levels [Eqs. (4.5)–(4.7)]. This $J(\omega)$ curve is linear in the absorption edge region and the value of $\omega_0$ obtained for a 10-at.% Cu alloy for example is the $\omega_0$ value for pure Ag, within experimental uncertainties. For a 45-at.% Ag alloy, we find 2.14 eV for $\omega_0$ instead of 2.08 eV for pure Cu [using $J(\omega)$], i.e., a shift of 3% towards higher energies only. Therefore, in both cases, we observe practically no shift of the matrix absorption edge when adding Ag or Cu impurities.

### 3. *Optical-energy-loss function*

From the complex dielectric constant, the optical energy-loss function can be calculated

$$\mathrm{Im}(1/\epsilon) = \epsilon_2/(\epsilon_1^2+\epsilon_2^2)\,. \tag{3.7}$$

Peaks in $\mathrm{Im}(1/\epsilon)$ may indicate the existence of electronic collective oscillations. However, plasma oscillations at $\Omega_p$ do exist only if the two following conditions are simultaneously satisfied:

$$\epsilon_1(\Omega_p) = 0\,, \tag{3.8a}$$

$$\epsilon_2(\Omega_p) \ll 1\,. \tag{3.8b}$$

It must immediately be noted that this plasma frequency $\Omega_p$ is different from the frequency $\omega_p$ introduced in the Drude region for the conduction electron gas by $\omega_p^2 = 4\pi Ne^2/m^*$, because the plasma frequency is shifted towards smaller energies by the presence of interband transitions. One can indeed write

$$\epsilon_1(\omega) = 1 - \omega_p^2/\omega^2 + 4\pi\alpha_0 + \delta\epsilon_1^{(i)}(\omega)\,. \tag{3.9}$$

$\Omega_p$ will be defined by $\epsilon_1(\Omega_p) = 0$, i.e.,

$$\Omega_p = \omega_p/[1 + 4\pi\alpha_0 + \delta\epsilon_1^{(i)}(\Omega_p)]^{1/2} \ll \omega_p\,. \tag{3.10}$$

For pure Au and Au-rich alloys and pure Cu and Cu-rich alloys, one cannot find $\omega$ values for which the conditions (3.8) are satisfied, even though

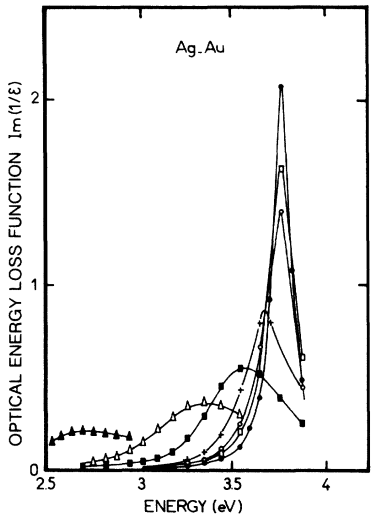


FIG. 7. Optical energy-loss function $\mathrm{Im}(1/\epsilon)$ vs energy for Ag-Au alloys with Au concentrations in at.%: 2 (□), 3 (○), 6 (+), 14 (■), 30 (△), 84 (▲) and for pure Ag (●).

$\mathrm{Im}(1/\epsilon)$ shows a peak in the energy range under consideration; true plasma oscillations do not exist in these cases. On the contrary, for pure Ag and Ag-rich alloys, a plasma frequency can be defined. For pure Ag,[31] $\mathrm{Im}(1/\epsilon)$ presents a very sharp peak at $\Omega_p = 3.77$ eV, which is to be compared with $\omega_p = 9.6$ eV (corresponding to $m^* = 0.89m$). For *Ag*-Au alloys,[35] the peak of $\mathrm{Im}(1/\epsilon)$ moves towards smaller energies with increasing Au concentration as seen in Fig. 7; at the same time, its height decreases and its width related to $\epsilon_2(\Omega_p)$, increases. This means that plasma oscillations become more and more damped on alloying, which can be explained by the increase of $\epsilon_2(\Omega_p)$, related to the shift of the interband transition onset towards lower energies.

Figure 8 shows the behavior of $\mathrm{Im}(1/\epsilon)$ in *Ag*-Cu alloys, for which the absorption onset is roughly the one of pure Ag, but a supplementary absorption peak appears around 3.2 eV. The peak of $\mathrm{Im}(1/\epsilon)$ moves only slightly towards higher energies with respect to its position in pure Ag and the shift seems to be about the same for all concentrations, probably because of the balance of different effects. As in the *Ag*-Au case, the peak intensity decreases and its width increases with increasing impurity concentration.

## B. Ordered phases

The Au-Cu phase diagram is the only one which exhibits the presence of ordered phases, over composition ranges corresponding to $AuCu_3$, AuCu, and $Au_3Cu$. The $Au_3Cu$ ordered phase can be ob-

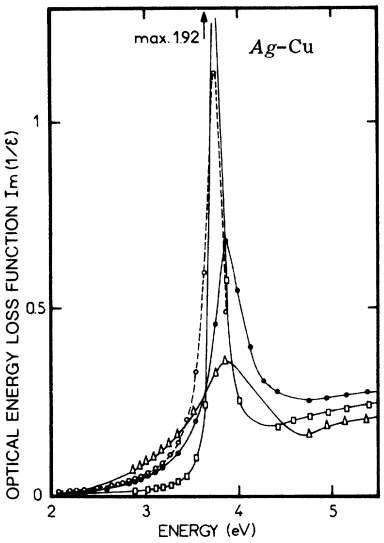


FIG. 8. Optical energy-loss function $\mathrm{Im}(1/\epsilon)$ vs energy for *Ag*-Cu alloys with Cu concentrations in at.%: 8 (●) and 30 (△), for pure Ag (□) and the Ag–8-at.%-Cu alloy after annealing (○).

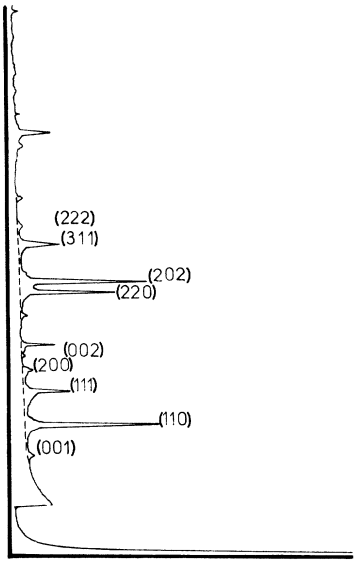


FIG. 9. Microdensitometer analysis of an electron diffraction diagram of a Au–54-at.%-Cu alloy, partially ordered according to AuCu (I).

tained only after very long annealing times: about 100 to 200 h at 200 °C (Ref. 36); moreover, the ordered domains remain very small. Larger antiphase domains (350 Å) were produced when introducing a supersaturation of vacancies in bulk samples quenched from high temperatures.[37,38] Therefore, we considered only the $AuCu_3$ and AuCu ordered phases (forms I and II). The structure of AuCu (I) is face-centered tetragonal. The structure of AuCu (II) is orthorhombic and closely related to the AuCu (I) structure.[39] It can be thought of as consisting in ten tetragonal cells side by side, with Cu and Au atoms reversing positions after five cells. The superlattices $AuCu_3$ (I) and (II) are fcc and II is related to I as in the previous case.

The analysis of electron diffraction diagrams permits the identification of the phase constituting the alloy film, and, in the case of ordered phases, a determination of the degree of order. Figure 9 shows the microdensitometer analysis corresponding to a 54-at.% Cu alloy annealed at 390 °C; it exhibits two superlattice rings: (001) and (110), attributed to AuCu(I). In the case of AuCu(II), the (110) ring would be split into two satellite rings: (190) and (1 11 0).[40] If the film consists of a mixture of I and II, the two satellites appear on either side of the (110) ring.[22]

In order to evaluate the degree of order in our films, we used the Bragg-Williams definition[41] of the long-range order parameter $S$,

$$S=(n-p_A)/(1-p_A)\,, \tag{3.11}$$

where $p_A$ is the fraction of $A$ atoms which occupy $\alpha$ lattice sites for perfect order and $n$ is the fraction of $\alpha$ sites actually occupied by $A$ atoms. $S$ equals zero for total disorder and equals one for perfect order. The $S$ parameter is related to the intensities of a superlattice ring $I_S$ and a normal ring $I_N$ by

$$S^2=(I_S/I_N)_{\mathrm{expt}}\,(I_N/I_S)_0\,, \tag{3.12}$$

where $(I_S/I_N)_{\mathrm{expt}}$ is the measured intensity ratio between the rings $S$ and $N$, and $(I_S/I_N)_0$ is the intensity ratio computed for perfect order. This relation was established for alloys with the stoichiometric composition corresponding to the superlattice. For alloys with different compositions, we used the same expression for determining $S$, although the maximum order in these cases does not correspond to $S=1$, but to an $S_{\max}$ smaller than 1 and depending on the composition.

### *1. $AuCu_3$ superlattice*

We investigated several alloys with compositions close to the stoichiometric composition. Figure 10 shows the variation of the imaginary part of the total dielectric constant $\epsilon_2(\omega)$ versus energy for a 81-at.% Cu alloy, in disordered state and at different degrees of ordering. The curves are arbitrarily shifted with respect to each other and displayed according to increasing degree of order. Neither the absorption edge nor the first maximum in $\epsilon_2$ (Cu-like) seem to be much affected by ordering. By contrast, the high energy part of the curve is appreciably modified, its shape changing gradu-

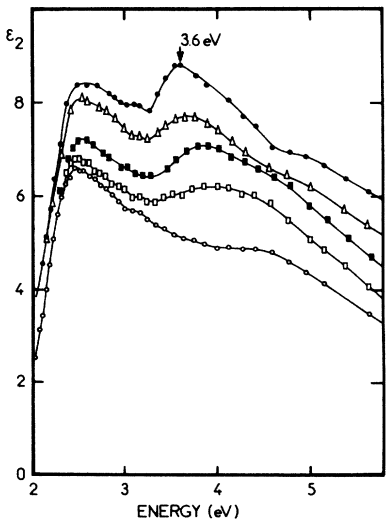


FIG. 10. Imaginary part of the dielectric constant $\epsilon_2$ vs energy for a Au–81-at.%-Cu alloy, first disordered (○), then partially ordered according to $AuCu_3$ (□, ■, △, ●) with increasing degrees of order [maximum order (●)].

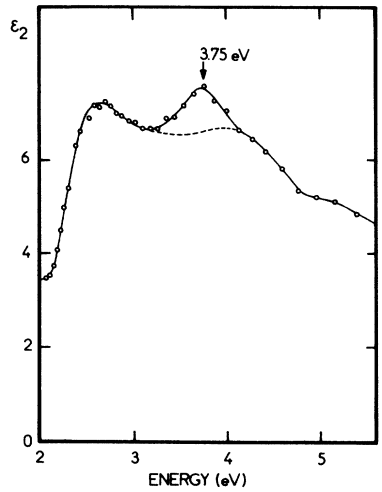


FIG. 11. Imaginary part of the dielectric constant $\epsilon_2$ vs energy for a Au–54-at.%-Cu alloy, partially ordered according to AuCu (I) (○) and disordered [interpolated (---)].

ally from the completely disordered state to the state of maximum order. For a small degree of order, a supplementary absorption arises as a broad peak centered at about 4 eV. When the degree of order increases, this peak becomes narrower and moves towards smaller energies. Simultaneously, a small peak seems to appear at about 5 eV. For maximum order, there is a well-defined additional peak centered at 3.6 eV. Such a feature characteristic of the ordered phase, located at about 3.5 eV, was observed by Stahl *et al.*[13] and Nilsson *et al.*[12] (the supplementary absorption mentioned by Stahl *et al.*[13] between 0.68 and 2 eV does not appear in our films). Slightly different results were obtained by Scott and Muldawer,[14] who found the additional absorption at 3.28 eV for bulk polished samples.

### 2. *AuCu superlattice*

The AuCu ordered phase exists in a wide concentration range, between 35- and 65-at.% Cu. Near the stoichiometric composition, the AuCu (I) phase is formed; away from it, either phase I or phase II, and more likely a mixture of both, are found. Figure 11 shows the spectrum of $\epsilon_2$ versus energy for a 54-at.% Cu alloy ordered according to AuCu (I). The $\epsilon_2$ curve corresponding to the disordered phase (discontinuous line), obtained by interpolation from the curves for disordered alloys with various compositions, has been drawn for comparison. The well-defined maximum centered at 3.75 eV must, without ambiguity, be attributed to the presence of compositional order. Films ordered according to AuCu (II) give a similar result, but the absorption peak seems broader.

In conclusion, ordering has a strong effect on that part of the optical absorption which is due to interband transitions. It is accompanied by the appearance of a new absorption peak, centered at about 3.6 eV for $AuCu_3$ and 3.75 eV for AuCu. By contrast, the onset of interband transitions is not modified by ordering.

### C. Nonhomogeneous alloys; Phase separation effects

Since the mutual solubility of Ag and Cu is very small, Ag-Cu solid solutions can only be obtained in a metastable state and they show a strong tendency towards segregation. Therefore, careful structure studies are absolutely necessary before interpreting the optical properties. In order to obtain true Ag-Cu solid solutions, the films must be deposited on cold substrates (80–120 °K). These films are found to be microcrystalline when warmed up to room temperature.[23] Between 35- and 65-at.% Cu, Mader[42] claimed to obtain amorphous films, but in fact samples in the concentration range around 50 at.% often consist of several phases: alloy, pure Ag and pure Cu.[43]

Figure 12 illustrates the influence of homogeneity on the optical properties by comparing the results obtained for two Ag-Cu alloy films with about the same concentration, but deposited and heat-treated in different ways. Curve 1 shows the variation of $\epsilon_2$ with frequency for a 30-at.% Cu alloy deposited on a substrate held at 120 °K and measured optically at room temperature. The optical absorption

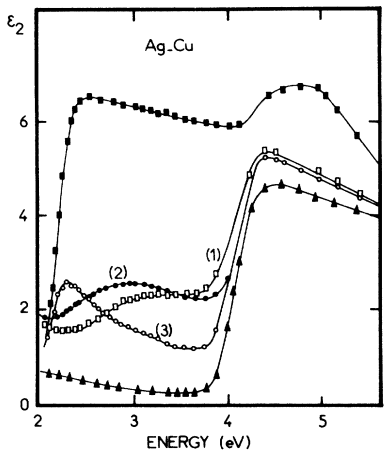


FIG. 12. Imaginary part of the dielectric constant $\epsilon_2$ vs energy for a Ag–30-at.%-Cu alloy deposited on a substrate at 120 °K [curve 1, (□)], a Ag–29-at.%-Cu alloy deposited on a substrate at room temperature [curve 2, (●)], the Ag–30-at.-Cu alloy after annealing at 600 °K [curve 3, (○)] and for pure Cu (■) and pure Ag (▲).

of this film corresponds to the case described previously and can be analyzed as reported in Sec. IV in the framework of the virtual bound state model. Curve 2 corresponds to a 29-at.% Cu film deposited on a substrate at room temperature: the additional absorption related to Cu impurities has a different shape and is shifted towards smaller energies. The optical absorption of this film cannot be fitted to a virtual-bound-state expression. Curve 3 represents $\epsilon_2(\omega)$ for the first 30-at.% Cu film after annealing at about 300 °C. This latter curve consists of two distinct parts. Between 2 and 2.5 eV there is a peak corresponding to the first maximum in $\epsilon_2(\omega)$ for pure Cu, following an absorption edge located at the same position as in pure Cu. At about 4 eV there is a second absorption edge very similar to that of pure Ag which is only slightly modified with respect to curve 1 (before annealing). It must be noted that, in the case of annealing films, the $\mathrm{Im}(1/\epsilon)$ curve exhibits a sharp peak at the same position as in pure Ag (Fig. 8 for an 8-at.% Cu alloy film).

The structure and homogeneity of the alloy films have been thoroughly investigated in each case. Curve 1 corresponds to a true solid solution (30-at.% Cu): the electron diffraction pattern exhibits a (111) peak which corresponds to a 35-at.% Cu alloy. It, however, also shows the presence of a few domains of pure Ag which are small enough to be ignored optically. Curve 2 corresponds to a partially phase-separated alloy: one obtains essentially the diffraction pattern of the matrix (pure Ag), because the Cu atoms do not yet form clusters large and well oriented enough to give observable diffraction rings. In the case of curve 3, phase separation is complete and the diffraction pattern consists of the superposition of the two patterns of pure Cu and pure Ag. The electron micrographs show large dark areas which were attributed to Cu microcrystallites formed at the film surface after migration of Cu atoms, probably along grain boundaries. For a 50-at.% Cu film after annealing, it was possible to detect a "Moiré" ring and "Moiré" fringes suggesting that these Cu crystallites may grow on the top of some Ag crystallites and in epitaxy with them.[23]

In conclusion, these experiments indicate that, at least for *Ag*-Cu alloys, the optical properties are very sensitive to local atomic environment.

## IV. DISCUSSION AND INTERPRETATION

### A. Disordered alloys

Our results on disordered systems will be essentially interpreted according to the CPA.[1,2] However, for *Ag*-Cu alloys, we will use a model based on the virtual-bound-state theory, proposed by Friedel[4] and Anderson,[5] which gives a better description of charge screening around the impurity and allows a quantitative analysis of the optical results.

The CPA is a method valid for binary alloys $A_xB_{1-x}$, which has recently been developed in order to palliate the inadequacies of the rigid band and the virtual crystal theories. In the rigid-band theory, the density-of-states function does not vary with concentration; the only alloying effect is the displacement of the Fermi level due to the variation in electron concentration. The virtual crystal theory describes the alloy as an ordered medium, whose potential is the mean potential: $V = xV_A + (1-x)V_B$, where $V_A$ and $V_B$ represent the potentials on sites $A$ and $B$ respectively. These approximations are only justified in the weak-perturbation limit, i.e., if the difference in potential of the two constituents is small compared to their bandwidth. These theories cannot give a correct description for alloys of transition metals and noble metals, for which the difference in potential may be of the order of the halfwidth of the $d$ band.

The CPA represents the alloy, not by a mean potential, as in the virtual crystal theory, but by an effective potential $\Sigma$ determined in a self-consistent way: the mean density of states in the alloy $g(E,\Sigma)$ must be equal to the average of the partial densities of states corresponding to an atom $A$ or $B$ embedded in this effective medium:

$$g(E,\Sigma) = xg_A(V_A,\Sigma) + (1-x)g_B(V_B,\Sigma). \qquad (4.1)$$

The degree of individuality of the partial bands in the alloy depends on the difference in potential between $A$ and $B$, and on the $d$-band width $2w$, taken to be the same for the pure metals. The important parameter is $\delta = (V_A - V_B)/w$; if $\delta$ is small, the total density of states tends towards the one corresponding to the virtual crystal model; if $\delta$ is large, the two partial densities are practically independent.[2] It must be emphasized that, in the case of noble metals, where the $d$ band is coupled to the $s$ band, the limit case of separate bands is never reached. If the $d$ band widths of the pure metals are very different, one has also to consider the off-diagonal disorder characterized by the ratio of the two $d$-band widths $w_A/w_B$.[44,45] This effective potential $\Sigma$ is energy dependent and complex; its imaginary part, representing the damping of the electron states due to disorder can generally be related to the reciprocal-relaxation time.[46] The CPA can be generalized to account for charge transfers which determine the variation of the $V_A$ and $V_B$ potentials with concentration, and also for local environment effects.[47]

The CPA was first applied to the computation of the optical conductivity for binary alloys, using a one-band tight-binding model to represent each constituent.[48] This model does not give a correct approximation for noble metals. Levin and Ehrenreich[49] then proposed a two-band model, in which a tight-binding $d$ band is coupled to a conduction band by a hybridization interaction, which permits the computation of the $s$ and $d$ densities of states. This model was applied to Au-Ag alloys and was used to determine, from the $d$ density of states in the alloys, the variation with concentration of the onset of interband transitions, which indeed corresponds to transitions between the top of the $d$ band and the Fermi level. Subsequently, Gelatt and Ehrenreich[17] modified this treatment in order to eliminate some nonphysical features entering the former version. These authors emphasized the importance of a correct evaluation of the relative positions of the Fermi levels ($E_F$) of the two constituents, as well as of the positions and the widths of their $d$ bands, in order to determine the charge transfers between both types of atoms in the alloy. They suggested to consider the vacuum level as a reference level, and to set: $E_F = -\Phi$, where $\Phi$ is the electron work function. In Fig. 13, we propose a scheme of the relative positions of $d$ bands in the three series of alloys, using the suggestion of Gelatt and Ehrenreich with the help of the values reported in Table IV. The values of $\Phi$ are taken from Ref. 50, the energy $E_0$ between the top of the $d$ band and the Fermi level $E_F$ is deduced from our optical measurements, the $d$-band widths $2w$ are obtained by x-ray photoemission-spectroscopy (XPS)[51] and ultraviolet-photoemission-spectroscopy (UPS)[52] measurements.

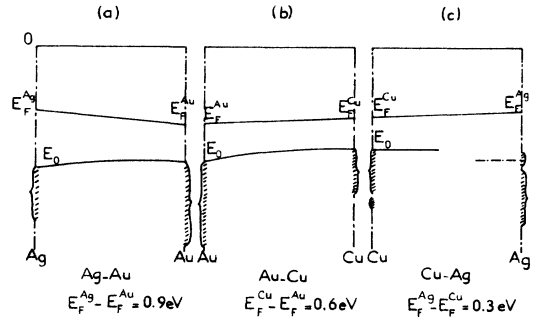


FIG. 13. Schematic picture of the variation with composition of the Fermi level $E_F$ and the $d$-band top energy $E_0$ for Ag-Au (a), Au-Cu (b), Cu-Ag (c) alloys; the $d$-bands widths for the pure metals are also indicated.

The amount of total charge transfer between the two constituents can be related in a semiempirical way to the difference in their work functions, i.e., in the positions of their Fermi levels.[53] Consequently, a difference $E_F^{Ag} - E_F^{Au} > 0$ should imply a total charge transfer from Ag to Au, a difference $E_F^{Cu} - E_F^{Au} > 0$, a total charge transfer from Cu to Au. As $E_F^{Ag} - E_F^{Cu}$ is very small and positive, the total charge transfer in this case is expected to occur from Ag to Cu, but it should be small. On the other hand, the values of the electronegativity (according to Pauling's scale) are 1.9 for Ag and Cu, 2.4 for Au. Au being more electronegative than Ag and Cu, a total charge transfer from Ag to Au and from Cu to Au seems reasonable; on the contrary, Ag and Cu having the same electronegativity, one expects small charge transfer, which will be related to a change in band shapes rather than to the difference of Fermi energies.[17] Experimental evidence of charge transfers is provided by Mössbauer isomer-shift measurements on $^{197}$Au. The observed shift is 2.2 mm sec$^{-1}$, when introducing 1-at.% Au in Ag, 4 mm sec$^{-1}$ when introducing the same quantity of Au in[54] Cu; in this latter case, the results must be corrected for volume effects. The schemes drawn using the values of Table III [Figs. 13(a)–13(c)] show a total overlap of $d$ bands in the Ag-Au case, a less

TABLE IV. Work function $\Phi$, $d$-band top energy $E_0$ (with respect to the Fermi energy $E_F$), $d$-band width $2w$ for Au, Ag, Cu.

| | Cu | Ag | Au | References |
|---|---|---|---|---|
| $\Phi$ (eV) | 4.6 | 4.3 | 5.2 | 50 |
| $(E_F - E_0)$ eV | 2.1 | 3.9 | 2.5 | this work |
| $2w$ (eV) | 3 | 3.5 | 5.7 | 51–52 |

complete overlap of $d$ bands in the Au-Cu case, but a very small overlap in the Ag-Cu case. In Ag-Cu alloys, by contrast to Au-Ag and Au-Cu, we must expect, at least in the dilute cases, two distinct $d$ bands.

A satisfactory picture of the $d$ density of states can be deduced from high-energy UPS experiments (40.8 eV). The spectra obtained by Mac Lachlan *et al.*[55] for a series of Au-Ag alloys show indeed a common $d$ density of states, which changes its shape and position when the Ag concentration increases. The first peak related to the Au partial density of states moves towards higher energies, while a peak related to the Ag partial density of states appears between 4 and 5 eV at concentrations higher than 25 at.%. The Au peak still exists for an Ag concentration of 75 at.%, while the Ag peak becomes more pronounced and moves slightly towards lower energies. By contrast, the curves deduced from UPS experiments by Shevchik and Goldmann[56] on Ag-Cu alloys give evidence for a different behavior, as expected. When Cu is added to Ag, the main Ag peak around 4 eV is broadened, but stays roughly at the same position as in pure Ag (there is only a very slight displacement towards higher energies), while a distinct additional peak appears at about 3 eV. Except for this peak and broadening effects, the curve is the same as for pure Ag up to 20 at.%. For higher Cu concentrations (56 at.%), the peak grows in intensity and broadens, and around 5.5 eV a structure attributed to Ag begins to emerge. For 89-at.% Cu, the curve is the same as for pure Cu, except for a structure which has emerged between 5 and 7 eV and which is associated with Ag. The peak observed at 3 eV corresponds to the partial density of states of Cu impurities in an Ag matrix, i.e., in terms of the virtual-bound-state model, to the resonance level of Cu in Ag. For Cu-rich alloys, there must be, in the same way, virtual bound states localized on Ag impurities, located in energy below the Cu $d$ band. The observed splitting of the Ag level might be explained by spin-orbit coupling as suggested by Shevchik and Goldmann.[56]

### *1. Interband transitions*

From the relative positions and the widths of the $d$ bands for pure metals, it is possible to understand qualitatively most of the experimental results. The striking differences observed between Au-Ag and Au-Cu on one hand, Ag-Cu on the other hand, suggest that these two cases be discussed separately.

The onset of interband transitions is attributed in Au and Cu to transitions between the top of the $d$ band and the Fermi level in the vicinity of $L$, with, in the Au case, a small contribution of transitions of the same type at $X$.[57-60] From piezo-optical measurements, as well as from experiments at different temperatures, it may be inferred that the absorption edge in pure Ag is composite. As for the other noble metals, it would be due partly to transitions from the top of the $d$ band to the Fermi level, partly to transitions between conduction bands at $L$ ($L_{4'} \rightarrow L_{4^+}$). Let us assume that in the three series of alloys, the absorption edge also corresponds essentially to transitions from the top of the $d$ band to $E_F$.

For Au-Ag alloys, the charge transfers and the resulting variation of the energy levels of Ag and Au with concentration have been calculated.[17] The results are shown in Fig. 14, after Brouers *et al.*[46] Since the $d$ states of Ag in pure Au lie deeper in energy than the Au $d$ states, Ag impurities in Au will only slightly modify the top of the $d$ band of the Au matrix. In the opposite case, the $d$ states of Au in pure Ag lie higher than the Ag $d$ states and Au impurities in Ag will strongly perturb the top of the $d$ band of the Ag matrix, leading to an appreciable shift of the absorption edge. For Au-Cu alloys, in the absence of any evaluation of charge transfers, the variation of the Au and Cu levels with concentration is not known; if we assume a roughly linear variation parallel to the $E_F(x)$ variation (Fig. 13), then we find, according to the same arguments as before, that the Au partial density of states must modify the top of

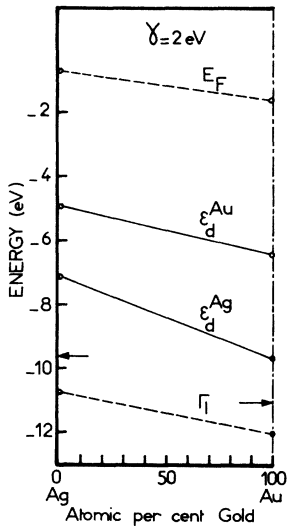


FIG. 14. Energy levels of Au, Ag, and $Au_xAg_{1-x}$. The broken lines refer to CPA results for $E_F$ and $\Gamma_1$ bottom of the hybridized $s$ band (the arrows indicate the bottom of the unhybridized $s$ band). The $s$ half band width $w_s$ is equal to 7 eV and the hybridization constant is $\gamma = 2$ eV for both metals [after Brouers, Brauwers, and Rivory (Ref. 46)].

the matrix $d$ band in $Cu$-Au alloys very slightly. On the other hand, the Cu partial $d$ density of states will perturb the top of the matrix $d$ band in $Au$-Cu alloys more strongly.

These interpretations are in complete agreement with the observed variation of the absorption edge for Au-Ag and Au-Cu alloys (Fig. 6). It must be emphasized here that the situation is in fact more complicated than explained above in the Au-Cu case, due to volume effects. Changes in electronic structure are indeed expected not only from potential differences, but also from variations of lattice constant. Such effects have been taken into account by Beaglehole and Erlbach[16] in the analysis of their differential results on dilute alloys.

The peak observed at about 5 eV in the optical absorption of pure Cu is composite. It is attributed to critical point transitions between conduction bands at $L$ ($L_2'\rightarrow L_1^u$) at about 4.3 eV and to transitions from the bottom of the $d$ band to the conduction band at the Fermi level in the vicinity of $L$ [$L_1\rightarrow E_F(L_2')$] at about 4.8 eV. Optical measurements at different temperatures[61] show that transitions between conduction bands are more sensitive to temperature than transitions from the $d$ band. Such a decomposition of this absorption peak is confirmed by computations of the dielectric constant, accounting for matrix element effects, by Janak *et al.*[62] As previously described, this peak moves to lower energies and disappears rapidly when adding Au to Cu. According to the results of measurements at different temperatures,[61] the corresponding volume effect (lattice dilation) must indeed produce a shift of the absorption peak towards lower energies. On the other hand, the contribution of transitions between conduction bands is expected to be strongly affected by disorder; the contribution of transitions from the bottom of the $d$ band to $E_F$ will also be affected by alloying, as suggested by the energy band scheme of Fig. 13(b), the bottom of the Cu $d$ band being strongly perturbed by the addition of Au impurities.

The origin of the optical absorption maximum in Au between 3.5 and 4.5 eV is more controversial; it must also be composite. One part may be attributed, as for Cu, to transitions between conduction bands at $L$ ($L_2'\rightarrow L_1^u$), another part to transitions between the top of the $d$ band and the first conduction band at $X$ ($X_5\rightarrow X_4'$) in nonrelativistic notations), as suggested by various differential experiments.[59,61,63] However, the contributions of transitions at critical points to the static optical spectrum are expected to be weak and obscured by large background coming from transitions involving the $d$ states and concerning extended regions in the Brillouin zone.[58,64] In the absence of computation of the different matrix elements, it is difficult to be certain. It should be noted that the Au spectrum in this energy range remains remarkably unchanged on alloying with Ag or Cu up to quite high impurity concentrations (up to 40 at.% in the case of Cu).

As previously emphasized, the Ag and Cu $d$ bands are narrow and separated in energy enough, so that the $d$ densities of states of each constituent are expected to keep their individuality in the alloys. The density of states of Cu impurities in an Ag matrix is centered at about 3 eV below the Fermi level, i.e., above the Ag $d$ band, whereas the Ag partial density of states in a Cu matrix lies around 5.5–6.5 eV,[56] i.e., below the Cu $d$ band. Therefore, we can understand why, for $Cu$-Ag alloys as well as for $Ag$-Cu alloys we observed the absorption edge of pure metals, Cu and Ag respectively, up to 10% impurities. For more concentrated alloys, for example in the case of a 45-at.% Ag alloy, a shift of the absorption edge corresponding to Cu of only 3% towards higher energy was found. This shift may be explained by assuming that the width of the Cu partial $d$ density of states decreases when increasing impurity (Ag) concentration, so that the distance between the top of the Cu $d$ band and the Fermi level increases slightly. In the case of $Ag$-Cu alloys (above 10-at.% Cu), we observed a broadening of the Ag matrix absorption edge as the Cu concentration increased, but we could not determine exactly the value of the absorption onset. Shevchik and Goldmann[56] report a 0.2-eV shift of the Ag density of states peak towards higher energies for a 20-at.% Cu alloy, which can also be due to a decrease in width of the Ag partial density of states.

It is interesting to consider again the behavior of the second main peak of Cu around 5 eV on alloying with Ag. For a 6-at.% Ag alloy, this peak is still well defined, but shifted towards lower energies (centered at about 4.6 eV). Such a shift is also observed on alloying with Au, but in this case the peak intensity is simultaneously lowered. Arguments forwarded for $Cu$-Au alloys are probably valid for $Cu$-Ag alloys, except for the one concerning the contribution of transitions from the bottom of the $d$ band to the Fermi level. Indeed, the Ag impurity level located around 5.5–6.5 eV, i.e., below the Cu $d$ band, is not expected to affect the bottom of this band appreciably. On the other hand, the decreasing Cu $d$-band width with increasing Ag concentration is associated with a decrease of the distance between the bottom of the Cu $d$ band and the Fermi level. This may explain the shift to lower energies of the contribution of the corresponding transitions, without the washing out

effects.

For a quantitative analysis of the absorption due to Cu impurities in Ag, we used the virtual-bound-state theory introduced by Friedel[4] and Anderson.[5] We followed the intuitive treatment proposed by Beaglehole[65,66] using the expressions obtained by Caroli[67] and Kjöllerström.[68] Optical absorption due to impurities in these alloys must be related to two processes: resonant scattering of conduction electrons by Cu impurities which leads to a frequency-dependent modification of the relaxation time $\tau$ and excitation of impurity $d$ electrons towards empty conduction states and of host conduction electrons to empty impurity $d$ states above the Fermi level $E_F$.

It is assumed that the impurity $d$ density of states $n_d(E)$ has a Lorentzian shape, centered at $E_d$ (measured relatively to $E_F$) and with a half-width $\Delta$:

$$n_d(E) = (10/\pi)\Delta/[(E-E_d)^2+\Delta^2] \ . \tag{4.2}$$

The relaxation time in the alloy $\tau(\omega)$ is defined by

$$1/\tau(\omega) = 1/\tau_p + x/\tau_i(\omega) \ , \tag{4.3}$$

where $\tau_p$ is the relaxation time in the pure crystal, $x$ is the impurity concentration, and $\tau_i(\omega)$ is the relaxation time due to impurity scattering given by

$$\frac{1}{\tau_i(\omega)} = \frac{1}{\tau_i(0)} \frac{E_d^2+\Delta^2}{2\Delta\omega} \times\left[\tan^{-1}\left(\frac{\omega-E_d}{\Delta}\right)+\tan^{-1}\left(\frac{\omega+E_d}{\Delta}\right)\right] . \tag{4.4}$$

This expression of $\tau(\omega)$ is then introduced in a generalized Drude formula giving the imaginary part of the dielectric constant due to intraband transitions of conduction electrons (including all scattering processes)

$$\epsilon_2^{(D)}(\omega) = \{\omega_p^2/\omega[\omega^2+\tau^{-2}(\omega)]\}[\tau(\omega)]^{-1} \ , \tag{4.5}$$

$\omega_p$ being the plasma frequency of the pure crystal ($\omega_p^2 = 4\pi Ne^2/m^*$). The interband transitions involving impurity states yield a contribution $\epsilon_2^{(ib)}(\omega)$,

$$\epsilon_2^{(ib)}(\omega) = x\left(\frac{\omega_d}{\omega}\right)^2 \times\left[\tan^{-1}\left(\frac{\omega-E_d}{\Delta}\right)+\tan^{-1}\left(\frac{\omega+E_d}{\Delta}\right)\right] , \tag{4.6}$$

where $\omega_d$ is the matrix element for $s$-$d$ transitions, assumed to be constant. The imaginary part of the total dielectric constant in the range $\omega<\omega_0$ ($\omega_0$ is the onset of interband transitions for pure Ag) is then given by

$$\epsilon_2(\omega) = \epsilon_2^{(D)}(\omega)+\epsilon_2^{(ib)}(\omega) \ . \tag{4.7}$$

The determination of the four main parameters $E_d$, $\Delta$, $\omega_d$, $[\tau_i(0)]^{-1}$ is obtained by a least-squares fitting of the experimental $\epsilon_2(\omega)$ or $\omega\epsilon_2(\omega)$ values.[69] This calculation requires knowledge of the values of the characteristic parameters of the matrix $\tau_p^{-1}$ and $\omega_p$. It is well known that $\tau_p^{-1}$ strongly depends on the structure of the thin films. Therefore, we performed several fittings with $\tau^{-1}$ values ranging from 0.025 to 0.05 eV, which account for the dispersion of the results obtained on pure Ag thin films. The choice of $\omega_p$ is still under discussion,[66] therefore $\omega_p$ was considered as a parameter. The results for $E_d$ and $\Delta$ depend only slightly on the values chosen for $\tau_p^{-1}$. By contrast, the values of $[\tau_i(0)]^{-1}$ and $\omega_p$ are dependent on this choice; moreover they are strongly correlated, as can be verified from an examination of the formula. The results for $E_d$, $\Delta$, and $\omega_d$ are shown in Table V for different concentrations. They represent the characteristic parameters of the $d$ virtual bound states localized on Cu impurities in an Ag lattice; the corresponding density of states is centered at 3 eV below the Fermi level and has a half-width at half-height of about 0.45 eV. Nilsson[15] noted in Ag-Cu alloys a supplementary absorption peak starting at 2.7 eV, which he attributed to the presence of Cu impurities, but he did not go further in the analysis of the data. We must emphasize again the very good agreement of our results with the UPS measurements by Shevchik and Goldmann,[56] which give evidence for the Cu $d$ density of states centered at about 3.3 eV below the Fermi level.

In Table V, the results corresponding to a 30-at.% Cu alloy are also given. It should be noted that the fitting is relatively poor in this limiting case, even if the values of the parameters are about the same as for more dilute alloys, for which the virtual bound state model is strictly valid.

It is interesting to compare the virtual bound state model, valid for a $d$ impurity embedded in a conduction electron sea with the more general

TABLE V. Position $E_d$ with respect to the Fermi energy, half-width $\Delta$, matrix element $\omega_d$, characterizing the virtual bound states localized on Cu impurities for different Ag–Cu alloys.

| $x_{Cu}$ | $E_d$ (eV) | $\Delta$ (eV) | $\omega_d$ (eV) |
|---|---|---|---|
| 0.06 | 3.1± 0.1 | 0.56± 0.06 | 4.4 |
| 0.08 | 3.0± 0.1 | 0.4 ± 0.1 | ••• |
| 0.09 | 3.15± 0.1 | 0.45± 0.1 | 3.6–4 |
| 0.10 | 3.1± 0.1 | 0.5 ± 0.1 | 4–5 |
| 0.30 | 3.0± 0.1 | 0.31± 0.05 | 3–4 |

CPA treatment for dilute alloys. The theory of the static electrical conductivity in disordered systems has been developed in the framework of the CPA using a two-band model by Brouers and Vedyayev.[70] In the dilute limit case, the $d$ density of states of an $A$ impurity ($\epsilon_d^A$ level) in a $B$ crystal ($\epsilon_d^B$ level) is expressed by

$$n_d^A(E) = (10/\pi)\Delta/[(E-E_d)^2+\Delta^2] \tag{4.8}$$

as previously, but with

$$\Delta = \tfrac{1}{2}\pi\gamma^2 n_{0s}[E-\gamma^2/(E-\epsilon_d^B)] , \tag{4.9a}$$

$$E_d = \epsilon_d^A + \gamma^2 R_e F_{0s}[E-\gamma^2/(E-\epsilon_d^B)] , \tag{4.9b}$$

where $\gamma$ is the $s$-$d$ hybridization constant, $n_{0s}$ is the $s$ density of states, and

$$F_{0s}(z) = \int_{-\infty}^{+\infty} n_{0s}(E)\,(z-E)^{-1}dE . \tag{4.9c}$$

$\Delta$ and $E_d$ are functions of energy and of the characteristics of the $B$ matrix. However, the $s$ density of states varies very little with energy and the $\gamma^2$ term in $E_d$ appears as a correction term. From the values of $\Delta$ given in Table V, and assuming a width of 14 eV for the $s$ band (value chosen for Au and Ag by Gelatt and Ehrenreich,[17] we can calculate the value of the hybridization constant $\gamma$. We obtain $\gamma = 1.5$ eV, which is in good agreement with the value generally used in computations. In the dilute case, the relaxation time can be expressed by

$$1/\tau(k) = 2\,|\,\mathrm{Im}\,\Sigma_s(E(k))\,| , \tag{4.10}$$

where $\Sigma_s$ is the self-energy. An effective matrix element for the $s$-$d$ scattering potential can be introduced

$$V_{s-d}^{\mathrm{eff}} = \gamma(\epsilon_d^A - \epsilon_d^B)/(E-\epsilon_d^B) . \tag{4.11}$$

The static relaxation time due to $A$ impurity can then be written

$$1/\tau_i = \pi(V_{s-d}^{\mathrm{eff}})^2 n_d^A(E_F) \tag{4.12}$$

in the same way as in Anderson's model. In this calculation, it is assumed that the width of the matrix $d$ band is only due to $s$-$d$ hybridization, which can be retained as long as effects outside the $d$ band are considered.

In practice, this calculation is valid for higher concentrations. The results obtained from these approximate formulas for the dilute case are in very good agreement with those obtained from complete formulas in the CPA up to concentrations of at least 15%.[71]

### 2. *Intraband transitions*

We reported earlier experimental evidence for a dependence of the optical relaxation time on frequency for all alloy compositions, according to

$$1/\tau(\omega) = 1/\tau(0) + b\omega^2 , \tag{4.13}$$

$b$ being a constant. The reciprocal relaxation time at zero frequency $[\tau(0)]^{-1}$ follows, as expected and like the dc electrical resistivity, a Nordheim-type variation with concentration

$$1/\tau(0) \propto x(1-x) . \tag{4.14}$$

The frequency dependence of the optical relaxation time exists for pure metals as well as for alloys and has been shown to be related to the sample structure in the case of pure metals.[27] Several explanations were proposed. Gurzhi[72] attributes this variation to electron-electron interaction. Nagel and Schnatterly[28] try to relate it to thin film structure by distinguishing two different regions: film areas where conduction electrons see a perfect lattice, i.e., inside the crystallites, and areas between crystallites (grain boundaries) where the lattice is strongly perturbed; they introduce a model with two kinds of carriers corresponding to these areas, which differ by their relaxation time. Brouers *et al.*[46] suggest that two mechanisms can lead to a $\omega^2$ variation of the reciprocal time: the scattering of conduction electrons due to imperfection disorder and to composition disorder effects on $d$ levels. The first process exists in pure metals as well as in alloys; the treatment accounts for the presence of imperfections in the film structure by assuming a fluctuation of $d$ levels from site to site with a Lorentzian distribution. The second process exists in alloys only and comes from the disorder effect on $d$ levels due to the difference in potential between the two constituents. In both cases, this $d$ disorder induces an indirect $s$ scattering through the $s$-$d$ hybridization interaction. The two types of disorder are treated within the CPA by generalizing the Velicky and Levin[48] formulation of the frequency-dependent conductivity to the two-band model. A frequency dependence of the reciprocal relaxation time as $\omega^2$ is indeed found, but no quantitative agreement with experimental results can be achieved. It is likely that various processes exist simultaneously and add their effects.

Theoretical calculations of the optical effective mass are more difficult, since they need a realistic representation of the velocity distribution and of the Fermi surface topology. Velicky and Levin[48] calculated the effective number of conduction electrons and the frequency dependent relaxation time for a single tight-binding band model, which is not able to represent the noble metal case correctly. They used expressions only valid for alloy constituents having identical band structure and found in all cases an increase of the optical mass on

alloying. Esterling,[73] using also a one-band model, showed the possibility for the optical mass to increase or decrease in dilute alloys, according to the relative positions and widths of the constituents. It seems necessary to use a two-band model, with correct values for the optical mass in pure metals; this is not possible in the simplified version of Brouers *et al.*,[46] where the *d*-band width comes from hybridization interaction only. A more sophisticated calculation is in progress.

### B. Au-Cu ordered alloys

As previously reported, optical absorption in an ordered alloy differs from that in a disordered alloy with the same composition only by the presence of a supplementary absorption peak, which is found at 3.6 eV for the $AuCu_3$ ordered phase and at 3.75 eV for the AuCu (I) ordered phase. The $AuCu_3$ ordered phase was optically studied by several authors[12,13] and their results are in good agreement with ours (except for Scott and Muldawer[14]).

Gray and Brown[74] computed the energy band structure for the $AuCu_3$ ordered phase and constructed the corresponding Fermi surface. Harrison[75] reached similar results by considering a $CuCu_3$ hypothetical phase, the band structure of which is obtained by folding the pure Cu one. The structure of the disordered phase, like the Cu one, is fcc, while the structure of the ordered phase is simple cubic; the corresponding Brillouin zone is also simple cubic and smaller than the disordered one; it thus introduces new Bragg planes. The $AuCu_3$ band structure along $\Gamma X$, for example, can be deduced from that of Cu, according to Harrison,[75] by folding the Cu one at the $\Gamma X$ middle point. Degeneracy, which was removed in Cu at $X$ $(X_4', X_1)$, is restored at $\Gamma$ after folding, but a new transition, from the Fermi level to a conduction band, is now allowed around 3.5 eV.

Therefore, the supplementary optical absorption appearing for the $AuCu_3$ or the AuCu ordered phases must be associated with new gaps opened in the band structure by the creation of new zone boundaries.

### C. Phase separation in Ag-Cu alloys

We already pointed out the differences observed in the optical absorption of Ag-Cu thin films deposited on substrates at different temperatures and submitted to different heat treatments, especially for Ag-rich alloys. Two limiting cases can be well characterized: on the one hand, true solid solutions, for which the Cu partial *d* density of states is centered at about 3 eV below the Fermi level (the optical absorption can then be analyzed in terms of the virtual-bound-state model), on the other hand, fully separated phases, with Cu atoms forming crystallites at the film free surface, for which the Cu partial *d* density of states has the same position with respect to the Fermi level, as in pure Cu. Partial phase separation was also observed: the position and shape of the optical absorption spectrum are then intermediate between these two limiting cases. We assume that Cu impurity atoms are able to migrate probably along grain boundaries and to rearrange themselves into clusters of like atoms.[23] These clusters remain, however, too small to be detected by electron diffraction until complete phase separation.

The influence of local atomic environment on partial *d* densities of states has recently been investigated, within an extension of the CPA, in transition metal binary alloys.[47] For example, the partial density of states of a given atom in an alloy is shown to depend appreciably on the configuration of nearest neighbors. Thus, the shape and the position of the local density of states corresponding to a particular cluster are different from those of the disordered alloy with the same concentration.

We have demonstrated that the optical absorption, at least in the case of Ag-rich alloys for which the spectrum is easy to analyze, appears to be quite sensitive to alloy homogeneity and show evidence for modifications of the impurity partial *d* density of states with atomic environment. A quantitative analysis of these data, however, remains difficult.

### ACKNOWLEDGMENTS

The author wishes to thank Professor F. Abelès, who suggested the present investigation, for his constant encouragements during the course of this work, Dr. M. L. Theye for many fruitful discussions and Dr. F. Brouers for his help and advice with the interpretation of the results. Suggestions and comments from Professor H. Ehrenreich are also gratefully acknowledged.

*Supported in part by the U. S. Dept. of the Army through its European office.

[1]P. Soven, Phys. Rev. 156, 809 (1967).
[2]B. Velicky, S. Kirkpatrick, and H. Ehrenreich, Phys. Rev. 175, 747 (1968).
[3]E. A. Stern, Phys. Rev. 144, 545 (1966).
[4]J. Friedel, Can. J. Phys. 34, 1190 (1956); Nuovo Cimento Suppl. 7, 287 (1958).
[5]P. W. Anderson, Phys. Rev. 124, 41 (1961).
[6]M. Hansen and K. Anderko, *Constitution of Binary Alloys* (McGraw-Hill, New York, 1958).
[7]P. R. Wessel, Phys. Rev. 132, 2062 (1963).
[8]H. Fukutani and O. Sueoka, *Optical and Electronic Structure of Metals and Alloys*, edited by F. Abelès (North-Holland, Amsterdam, 1966), p. 565.
[9]H. Fukutani, J. Phys. Soc. Jpn. 30, 399 (1971).
[10]A. J. McAlister, E. A. Stern, and J. C. McGroddy, Phys. Rev. 140, A2105 (1965).
[11]P. O. Nilsson, Phys. Kondens. Mater. 11, 1 (1970).
[12]P. O. Nilsson and C. Norris, Phys. Lett. A 29, 22 (1969).
[13]R. Stahl, H. J. Spranger, and H. P. Anbauer, Z. Metallkd. 60, 933 (1969).
[14]W. Scott and L. Muldawer, Phys. Rev. B 9, 1115 (1974).
[15]P. O. Nilsson and G. Forssell, J. Phys. (Paris) 35, C4-57 (1974).
[16]D. Beaglehole and E. Erlbach, Phys. Rev. B 6, 1209 (1972).
[17]C. D. Gelatt, Jr. and H. Ehrenreich, Phys. Rev. B 10, 398 (1974).
[18]H. Kiessig, Ann. Phys. (Leipz.) 10, 769 (1931). W. Umrath, Z. Angew. Phys. 22, 406 (1967).
[19]W. B. Pearson, *A Handbook of Lattice Spacings and Structures of Metals and Alloys* (Pergamon, New York, 1958).
[20]J. Philibert, J. Rivory, D. Bryckaert, and R. Tixier, J. Phys. D 3, L70 (1970).
[21]A. Guinier and R. Griffoul, Rev. Métall. 10, 387 (1948).
[22]J. Rivory, J. Phys. (Paris) 35, C4-51 (1974).
[23]J. Rivory, Thin Solid Films (to be published).
[24]F. Abelès and M. L. Theye, Surf. Sci. 5, 325 (1966).
[25]H. Ehrenreich and H. R. Phillip, Phys. Rev. 128, 1622 (1962).
[26]F. Abelès, *Optical Properties of Solids*, edited by F. Abelès (North-Holland, Amsterdam, 1972), p. 93.
[27]M. L. Theye, Phys. Rev. B 2, 3060 (1970).
[28]S. R. Nagel and S. E. Schnatterly, Phys. Rev. B 9, 1299 (1974).
[29]R. K. Linde, J. Appl. Phys. 37, 934 (1966).
[30]R. Stoering and H. Conrad, Acta Met. 17, 933 (1969).
[31]M. M. Dujardin and M. L. Theye, J. Phys. Chem. Solids 32, 2033 (1971).
[32]D. L. Martin and N. Waterhouse, Can. J. Phys. 48, 1217 (1970); D. L. Martin, *ibid.* 46, 923 (1968); A. Gavignet-Tillard and J. Hammann, Phys. Lett. A 37, 93 (1971).
[33]T. H. Davis and J. A. Rayne, Phys. Rev. B 6, 2931 (1972).
[34]H. Morinaga, Phys. Lett. A 32, 75 (1970); 34, 384 (1971).
[35]J. Rivory, Solid State Commun. 9, 1091 (1971).
[36]S. Ogawa and D. Watanabe, J. Phys. Soc. Jpn. 7, 36 (1952).
[37]D. Gratias and M. Condat, C. R. Acad. Sci. (Paris) 273, 336 (1971).
[38]P. M. Bronsveld and S. Radelaar, J. Phys. Soc. Jpn. 38, 1336 (1975).
[39]C. H. Johansson and J. O. Linde, Ann. Phys. (Leipz.) 25, 1 (1936).
[40]A. Pianelli, C. R. Acad. Sci. (Paris) 248, 2475 (1959).
[41]W. L. Bragg and E. J. Williams, Proc. R. Soc. Lond. A 145, 699 (1934). J. M. Cowley, Phys. Rev. 120, 1648 (1960).
[42]S. Mader, J. Vac. Sci. Technol. 2, 35 (1965). S. Mader, A. S. Nowick, and H. Widmer, Acta Met. 15, 203 (1967).
[43]G. Breitling, S. Mader, and H. Richter, Z. Naturfors. A 28, 1120 (1973).
[44]J. A. Blackman, D. M. Esterling, and V. F. Berk, Phys. Rev. B 4, 2412 (1971).
[45]M. Brauwers and F. Brouers, J. Phys. F (to be published).
[46]F. Brouers, M. Brauwers, and J. Rivory, J. Phys. F 4, 928 (1974).
[47]F. Brouers, F. Gautier, and J. van der Rest, J. Phys. F 5, 975 (1975); J. van der Rest, F. Gautier, and F. Brouers, *ibid.* 5, 995 (1975).
[48]B. Velicky and K. Levin, Phys. Rev. B 2, 938 (1970).
[49]K. Levin and H. Ehrenreich, Phys. Rev. B 3, 4172 (1971).
[50]D. E. Eastman, Phys. Rev. B 2, 1 (1970).
[51]I. Lindau and L. Wilson, Phys. Lett. A 42, 279 (1972).
[52]D. E. Eastman and J. K. Cashion, Phys. Rev. Lett. 24, 310 (1970).
[53]A. R. Miedema, F. R. de Boer, and P. F. de Chatel, J. Phys. F 3, 1558 (1973).
[54]P. H. Barrett, R. W. Grant, Morton Kaplan, D. A. Keller, and D. A. Shirley, J. Chem. Phys. 39, 1035 (1963).
[55]A. D. McLachlan, J. Liesegang, R. C. G. Leckey, and J. G. Jenkin, J. Phys. F 4, L253 (1974).
[56]N. J. Shevchik and A. Goldmann, in Proceedings of the Electron Spectroscopy Conference, Namur (1974) (unpublished).
[57]U. Gerhardt, Phys. Rev. 172, 651 (1968).
[58]N. E. Christensen and B. O. Seraphin, Phys. Rev. B 4, 3321 (1971).
[59]P. Szczepanek and R. Glosser, Solid State Commun. 15, 1425 (1974).
[60]M. Guerrisi, R. Rosei, and P. Winsemius, Phys. Rev. B 12, 557 (1975).
[61]G. P. Pells and M. Shiga, J. Phys. C 2, 1835 (1969).
[62]J. F. Janak, A. R. Williams, and V. L. Moruzzi, Phys. Rev. B 11, 1522 (1975).
[63]W. J. Scouler, Phys. Rev. Lett. 18, 445 (1967).
[64]B. R. Cooper, H. Ehrenreich, and H. R. Philipp, Phys. Rev. 138, A494 (1963).
[65]D. Beaglehole, Phys. Lett. A 40, 209 (1972).
[66]D. Beaglehole, J. Phys. F 5, 657 (1975).
[67]B. Caroli, Phys. Kondens. Mater. 1, 346 (1963).
[68]B. Kjöllerström, Philos. Mag. 19, 1207 (1969).
[69]J. Rivory, J. Phys. (Paris) 36, L-129 (1975).
[70]F. Brouers and A. V. Vedyayev, Phys. Rev. B 5, 348 (1972).
[71]F. Brouers (private communication).
[72]R. N. Gruzhi, Sov. Phys.-JETP 8, 673 (1959).
[73]D. M. Esterling, Solid State Commun. 15, 351 (1974).
[74]D. Gray and E. Brown, Phys. Rev. 160, 567 (1967).
[75]W. Harrison and M. B. Webb, *The Fermi Surface* (Wiley, New York, 1960), p. 28.